Fast charged-particle impact ionization of endohedral atoms

A. S. Baltenkov,[1] V. K. Dolmatov,[2] S. T. Manson,[3] and A. Z. Msezane[4]
[1]*Arifov Institute of Electronics, 100125 Tashkent, Uzbekistan*
[2]*Department of Physics and Earth Science, University of North Alabama, Florence, Alabama 35632, USA*
[3]*Department of Physics and Astronomy, Georgia State University, Atlanta, Georgia 30303, USA*
[4]*Center for Theoretical Studies of Physical Systems, Clark Atlanta University, Atlanta, Georgia 30314, USA*
(Received 21 November 2008; revised manuscript received 28 January 2009; published 10 April 2009)

The differential generalized oscillator strengths for ionization of the *s* subshells of He and Ne atoms encapsulated inside a fullerene, C_{60} cage, along with the single differential cross sections for ionization by fast electrons are calculated. The calculations have been performed using the two different model potentials to represent the fullerene shell. It is shown that the modulations of the wave function of the ejected electron caused by the interference between direct ejection and the waves scattered by the fullerene shell result in confinement resonances in the generalized oscillator strengths and the resulting impact-ionization cross sections. When the energy transfer to the target is close to that of the giant plasmon resonance in C_{60}, the interchannel interaction of the atomic ionization channels with the C_{60} ionization channels significantly influences the cross section for impact ionization of the confined atom. The formulas describing this interaction are derived and it is shown that for small momentum transfer this interaction is related to the dynamic polarizability of C_{60}. The general formulas are used to calculate impact ionization both of the He atom confined in C_{60} and of the empty C_{60} cage. The cross section of the latter process is compared to available experimental data.

DOI: 10.1103/PhysRevA.79.043201 PACS number(s): 36.40.Cg, 34.80.Gs

I. INTRODUCTION

The discovery that atoms can be encapsulated inside a fullerene [1] has stimulated significant activity within the scientific community. The static and dynamic properties of these new kinds of molecules, fullerene nanostructures, are novel and, thus, there has been great interest in studying them from a basic science point of view [2]. In addition, there are many possible applications of these caged-atom molecules that are being extensively pursued. For example, endohedral confinement can isolate the encapsulated atom from its environment, thereby serving as an elemental qubit for a quantum computer [3,4]; this isolation could also be employed in creative drug delivery schemes [5,6]. Moreover, the alteration of the properties of the confined atom by the surrounding fullerene alters the atomic properties [2], giving rise to the possibility of designing nanostructures with specific properties. All of these reasons, then, point to a rapid expansion of interest in the study of atoms endohedrally confined in fullerenes, particularly C_{60}.

The response of endohedral atoms to ionizing radiation, the process of photoionization, has been the subject of a large number of studies, primarily theoretical [7–16] but also some experimental [17,18]. However, the situation is different for electron-impact spectroscopy of endohedral atoms. To our knowledge, there are no reported theoretical or experimental investigations of charged-particle impact ionization of atoms, *A*, localized inside a C_{60} cage, generally denoted as $A@C_{60}$. At the same time the impact ionization of C_{60} fullerenes, i.e., the empty fullerene cages, by fast electrons is actively studied both experimentally [19–24] and theoretically [25,26]. There is a reason to believe that the electron-impact ionization studies of endohedral atoms will follow soon. In any case, to shed some light upon the role of the fullerene shell, C_{60}, in the charged-particle impact ionization of an encapsulated atom, we have initiated a theoretical program to investigate such collisions.

An essential factor limiting the possibility of electron spectroscopy is a necessity to separate a signal responsible for ionization of electrons under study (for example, electrons of the given atomic subshell) from a signal associated with the total current of electrons ejected from a target. In the case of endohedral atoms this problem is significantly simplified by the fact that the electronic subsystems of the fullerene shell and captured atom can be considered, under certain conditions and for a certain group of the encapsulated atoms [3,4], independently of each other. Therefore, comparison of the electron spectra of the $A@C_{60}$ molecules and empty C_{60} provides an opportunity to reliably separate a contribution of the electrons knocked out from the captured atom *A*.

When the energy transferred by a fast electron to the molecule $A@C_{60}$ is far from the characteristic energies of collective (or plasmon) electronic excitations of C_{60}, the fullerene shell can be considered, to an excellent approximation, as a static potential acting on the electrons of the encapsulated atom. When the transferred energy becomes closer to the energy of the plasmon excitations, the picture changes and the interaction of the electronic subsystems of the C_{60} and caged atom cannot be neglected. In the photoionization process, the giant dipole excitations of the C_{60} couple to the electrons of the endohedral atom and provide the dominant ionization mechanism in this energy range [15,16]; the same should be in evidence for ionization engendered by charged-particle-impact ionization.

In this paper we consider the both mechanisms for impact ionization of endohedral atoms, namely, impact atom ionization due to direct Coulomb interaction of fast electron with confined atom and ionization of this atom through coupling with plasmon excitations of C_{60}. The paper is laid out as follows. The principal expressions for the single differential

cross section (SDCS) and differential generalized oscillator strengths (GOSs) within the plane-wave Born approximation (PWBA) that are generally applicable to any spherically symmetric targets, including atoms localized in the center of a fullerene shell, are given in Sec. II. In Sec. III presented are the static model potentials approximating the effects of the fullerene cage and the limits of their applicability to describe endohedral atom impact ionization are defined. Section IV shows the calculated results for the impact ionization of the $1s$ and $2s$ levels of the Ne atom confined in C_{60} with the use of these potentials. Since the ionization energies of these levels are far from the energies of plasmon oscillations of C_{60}, the static potential approximation for GOS and SDCS calculations near the electron ejection thresholds is quite reasonable. The formulas describing endohedral atom impact ionization with dipole plasmon oscillations of C_{60} are derived in Sec. V. It is shown that for small momentum transfer, which dominates the impact-ionization process, the problem reduces to multiplying the dipole transition amplitudes by a screening function defined by the dynamical polarizability of C_{60}, just as in the case of endohedral atom photoionization [27]. The results are illustrated by calculations of the GOS for impact ionization of the $1s$ level of endohedral He. In Sec. VI the total cross section for impact ionization of the C_{60} molecule by fast electrons is calculated and compared to experimental data. Finally, Sec. VII gives our conclusions.

II. SCATTERING PROBLEM

Within the framework of the PWBA, valid for fast incident charged particles and small energy transfer, the SDCS $d\sigma_{nl_0}/d\varepsilon$ for the ionization of an atom, differential in the energy of the ejected (secondary) electron ε (or, equivalently, the energy loss of the impinging fast electron, $I_{nl_0}+\varepsilon=\Delta E$, where I_{nl_0} is the ionization potential of the atomic electron), is described by [28–30] the following expression (atomic units are used throughout this paper):

$$\frac{d\sigma_{nl_0}}{d\varepsilon}=\frac{16N_{nl_0}}{p_1^2k}\sum_{l,\lambda}(2l+1)(2\lambda+1)\times\begin{pmatrix} l_0 & l & \lambda \\ 0 & 0 & 0 \end{pmatrix}^2\int_{q_{\min}}^{q_{\max}}|Q_{l_0l}^{\lambda}|^2\frac{dq}{q^3}, \tag{1}$$

where k is the momentum of the electron ejected from the confined atom, N_{nl_0} is the number of electrons in the initial atomic nl_0 subshell, the symbol in brackets is the $3j$ symbol, and the matrix element, $Q_{l_0l}^{\lambda}$, is given by

$$Q_{l_0l}^{\lambda}(q)=\int_0^{\infty}P_{nl_0}(r)j_{\lambda}(qr)P_{kl}(r)dr. \tag{2}$$

The functions $P_{nl_0}(r)$ and $P_{kl}(r)$ are the radial parts of the one-electron wave functions for the initial $\varphi_i^a(\mathbf{r})$ and final $\varphi_f^a(\mathbf{r})$ states of the confined A atom, respectively, $j_{\lambda}(qr)$ is the spherical Bessel function [31], and $\mathbf{q}=\mathbf{p}_2-\mathbf{p}_1$ is the momentum transfer, where $\mathbf{p}_1$ and $\mathbf{p}_2$ are the momenta of the fast (primary) electron before and after collision with the atom. The upper and lower limits of the integral in Eq. (1) are

$$q_{\max}=p_1+p_2=p_1+\sqrt{p_1^2-2\Delta E},$$

$$q_{\min}=p_1-p_2=p_1-\sqrt{p_1^2-2\Delta E}. \tag{3}$$

The asymptotic behavior of the continuum wave function $P_{kl}(r)$ in Eq. (2) is given by

$$P_{kl}(r)_{r\to\infty}\to\sin\left(kr+\frac{1}{k}\ln 2kr-\frac{\pi l}{2}+\delta_l\right), \tag{4}$$

where δ_l is the phase shift.

The charged-particle impact-ionization process can also be characterized by the differential GOS [28,30], differential in the kinetic energy $\varepsilon=k^2/2$ of the secondary electron

$$\frac{df(q,\varepsilon)}{d\varepsilon}=\frac{4N_{nl_0}\Delta E}{\pi kq^2}\sum_{l,\lambda}(2l+1)(2\lambda+1)\begin{pmatrix} l_0 & l & \lambda \\ 0 & 0 & 0 \end{pmatrix}^2|Q_{l_0l}^{\lambda}(q)|^2. \tag{5}$$

In terms of the differential GOS, the single differential cross section, Eq. (1), is given by

$$\frac{d\sigma_{nl_0}}{d\varepsilon}=\frac{4\pi}{p_1^2\Delta E}\int_{q_{\min}}^{q_{\max}}\frac{df(q,\varepsilon)}{d\varepsilon}\frac{dq}{q}. \tag{6}$$

Thus, the single differential cross section is seen to be simply an integral over the differential GOS. It is useful to describe the ionization cross section in this form because the limit of the differential GOS, as the momentum transfer $q\to 0$, is the differential *optical* oscillator strength, which is proportional to the photoionization cross section [30]. Thus, investigation of the differential GOS gives insight into how the features seen in the photoionization cross section ($q=0$) are affected by the value of the momentum transfer and, as a result, how these features show up in the charged-particle impact-ionization cross section. Note that all of these PWBA expressions are generally applicable to any spherically symmetric targets, including endohedral atoms.

III. MODEL POTENTIALS OF THE FULLERENE SHELL

The fullerene cage is nearly spherical with a radius $R\approx 6.64$ a.u. [32]. The size of the empty cavity inside the cage significantly exceeds the extent of the ground-state wave function of an atom located at the center of the cage. Thus, in the matrix element of Eq. (2), the wave function of the nl_0 subshell in the initial state of the confined atom, $P_{nl_0}(r)$, is essentially the same as the corresponding free-atom wave function. The situation is different for the final-state continuum wave functions; since the continuum wave functions are of infinite extent; they are strongly impacted by the C_{60} cage potential. This results in interference between the ejected electron wave emerging directly and the waves scattered by the C_{60} cage potential; this interference gives rise to confinement resonances [11,12]. For small ejected electron energies, the wavelength $\lambda=2\pi/k$ significantly exceeds the distances between the carbon atoms forming the fullerene shell, so that the outgoing electron perceives the C_{60} cage potential as a uniform spherical layer of the

"smeared" carbon atoms. This electrically neutral layer can be well approximated as a short-range potential, $U(r)$, that represents the effect(s) of the fullerene shell on the confined atom. Within this framework, the calculation of the continuum wave functions reduces to solving the radial Schrödinger equation in which potential $U(r)$ is added to the free-atom potential.

There is, however, an important *caveat* in connection with this approximation; replacement of the C_{60} potential with a one-dimensional static potential $U(r)$ is reasonable only when the energy transferred to the endohedral atom by fast charged particle is far from the excitation energies of the giant plasmon resonance in the C_{60} shell itself at ~20 eV, and to a lesser extent, the much smaller plasmon resonance at ~40 eV, as is known from photoionization [15,16,33,34]. This is because in the vicinity of these plasmon resonances in the C_{60} cage, the ionization of the confined atom is strongly affected by the C_{60} plasmon resonances via interchannel coupling [16]. In Sec. IV we consider impact ionization of the Ne $1s$ and $2s$ subshells near their thresholds (roughly 900 and 50 eV, respectively) thereby insuring that the transferred energies ΔE do not overlap the plasmon excitations. In any case, as delineated above, within the range of transferred energy ΔE appropriate to Ne $1s$ and $2s$, the representation of the C_{60} shell potential as a static potential $U(r)$ is an excellent approximation.

In this paper two model potentials $U(r)$ for the fullerene shell are considered. The first, a spherical square-well potential [12], is defined as

$$U(r) = \begin{cases} 0, & \text{for } r \le R_0, \\ -U_0, & \text{for } R_0 < r < R_0 + \Delta, \\ 0, & \text{for } r \ge R_0 + \Delta. \end{cases} \tag{7}$$

Here R_0 is the inner radius of the cage potential, Δ is the thickness of the fullerene shell formed by the smeared carbon atoms, and U_0 is the potential-well depth. The potential parameters used are $R_0=5.8$ a.u., $\Delta=1.9$ a.u., and $U_0=8.4$ eV. These parameters result from a fit to experimental structural data for the empty C_{60} molecule and they reproduce the electron affinity of empty C_{60}: $I_{\text{ion}}=2.65$ eV [32]. With this model potential, the continuum wave functions $P_{kl}(r)$ for secondary electrons ejected from the caged atom are calculated in the one-electron approximation with addition of the model potential, Eq. (7), to the atomic Hartree-Fock potential

The second model potential of the fullerene shell, called the bubble (spherical δ function) potential [35–37], is defined by

$$U(r) = -B\delta(r-R), \tag{8}$$

where R is the mean shell radius, taken as 6.64 a.u. [32], and the parameter B is chosen to reproduce the experimental electron affinity of empty C_{60} which yields $B=0.442$ a.u. Introduction of this bubble potential, Eq. (8), into the Schrödinger equation simply introduces a multiplicative factor, $D_l(k)$, to the continuum wave function for the free atom. This factor depends upon both orbital angular moment l and k. Therefore, within the endohedral atom model based on the bubble potential of Eq. (8), the matrix element, Eq. (2), becomes

$$Q^{\lambda}_{l_0 l}(q) = D_l(k) \int P_{nl_0}(r) j_{\lambda}(qr) P_{kl}(r) dr, \tag{9}$$

with $P_{kl}(r)$ being the free A atom continuum wave function. The amplitude factor $D_l(k)$ can be expressed via the regular $P_{kl}(r)$ and irregular-at-zero $G_{kl}(r)$ solutions of the Hartree-Fock equations for the isolated atom [36,37]

$$D_l(k) = \cos\ \eta_l(k) \left[1 - \tan\ \eta_l(k) \frac{G_{kl}(R)}{P_{kl}(R)} \right], \tag{10}$$

where the additional phase shift $\eta_l(k)$ due to the potential well, Eq. (8), is defined by

$$\tan\ \eta_l(k) = \frac{P^2_{kl}(R)}{P_{kl}(R) G_{kl}(R) + k/2B}. \tag{11}$$

The irregular-at-zero wave function, $G_{kl}(r)$, in Eqs. (10) and (11) has the asymptotic form

$$G_{kl}(r)_{r\to\infty} \to -\cos\left(kr + \frac{1}{k} \ln 2kr - \frac{\pi l}{2} + \delta_l \right). \tag{12}$$

The logarithmic derivative jump, ΔL, at $r=R$ defines the parameter B through the relation $\Delta L = -2B = -\beta(1+\coth \beta R)$ [38], where $\beta = \sqrt{2I_{\text{ion}}}$.

IV. IMPACT IONIZATION OF Ne@C_{60}

The differential GOSs, $df/d\varepsilon$, were calculated for a variety of momentum transfers, q, for secondary electron energies ε up to 80 eV using modified versions of the codes of Ref. [39]. Eight partial waves with orbital angular momenta $0 \le l \le 7$ were taken into account in the summation of Eq. (5); the contribution of higher partial waves was negligible for the range of ejected electron energies considered here. The calculated results for the generalized oscillator strengths for the ionization of the $1s$ and $2s$ states of atomic Ne for Ne@C_{60} are presented in Figs. 1 and 2. Shown in each figure are the results calculated with each of the model potentials, along with the results for the free Ne atom for comparison.

The outstanding features of these results are the oscillations in the differential GOS, $df/d\varepsilon$, as a function of secondary electron energy, for both atomic levels and in both models of Ne@C_{60}, as compared to the free Ne results, i.e., confinement resonance structure. Moreover, it is seen that near the threshold the differences from the free-atom results are particularly dramatic. It is also evident that, with increasing secondary electron energy, the confinement resonances die out, with the spherical square-well potential result dying out much more rapidly (with energy) than the bubble potential result; in fact the bubble potential confinement resonances are more prominent at all energies, but this is accentuated with increasing energy. This difference occurs because the bubble potential involves interference between two waves, the direct ejected electron wave and the wave scattered off the C_{60} potential, while for the spherical square-

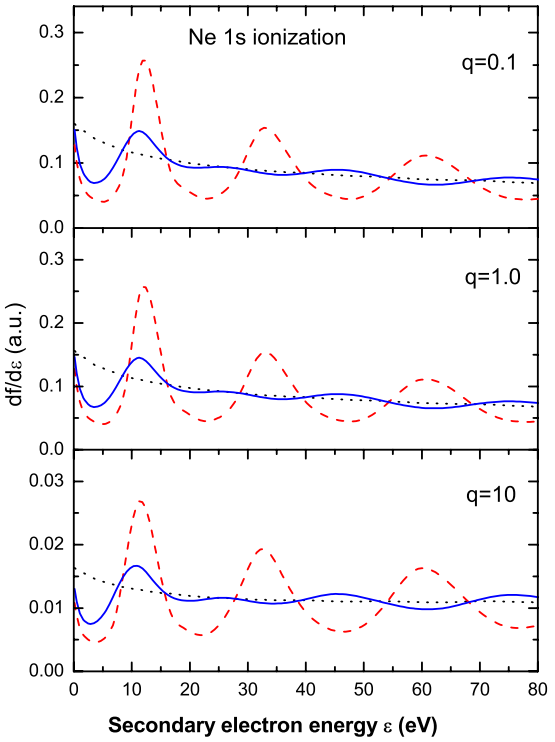

FIG. 1. (Color online) Differential generalized oscillator strengths calculated for ionization of Ne 1*s* of Ne@C_{60} as a function of ejected electron energy for several values of the momentum transfer q (in a.u.) using two different models of the cage potential: solid line—spherical square-well potential, dashed line—bubble potential. Also shown is the calculated result for free Ne atoms—dotted line.

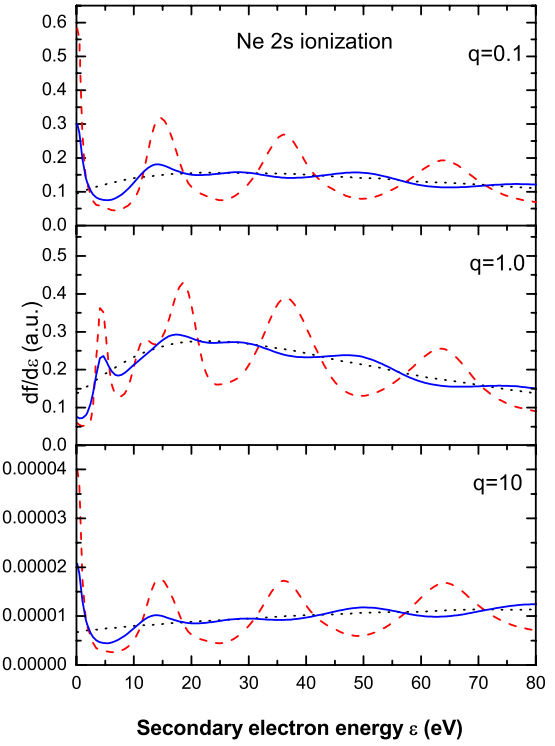

FIG. 2. (Color online) Differential generalized oscillator strengths calculated for ionization of Ne 2*s* of Ne@C_{60} as a function of ejected electron energy for several values of the momentum transfer q (in a.u.) using two different models of the cage potential: solid line—spherical square-well potential, dashed line—bubble potential. Also shown is the calculated result for free Ne atoms—dotted line.

well potential there are three interfering waves, namely, the direct and the scattered waves from the inner and outer edges of the potential. The bubble potential confinement resonances are more prominent than those generated by the spherical square-well potential for all energies because the two waves in the bubble potential model can be exactly in phase. Apparently, however, the three waves generated in the spherical square-well model are never completely in phase. As far as the decrease of the confinement resonances with energy is concerned, clearly the amplitude(s) of the scattered wave(s) diminishes with increasing energy. This is seen most easily for the bubble potential where the phases $\eta_l(k)$ approaches zero with increasing k, as seen from Eq. (11) so that $D_l(k) \to 1$ [Eq. (10)], i.e., the scattered wave becomes negligible. Sample calculations (not shown) using a much narrower (smaller Δ) spherical square-well potential, with U_0 adjusted to produce the correct electron affinity for C_{60}, tend toward the bubble potential results, indicating clearly that it is indeed the interference of three waves that accounts, in the main, for the differences between the two model potential results. A similar tendency was demonstrated in the calculated Ne 1*s*, 2*s*, and 2*p* photoelectron angular distributions from Ne@C_{60} [11] and the Xe 4*d* photoionization cross section of Xe@C_{60} [40].

Comparison of the evolution of the differential GOS results to momentum transfer for Ne 1*s* and 2*s*, shown in Figs. 1 and 2, illustrates the dependence of the results on the radius of the subshell being ionized in the confined atom. For Ne 1*s* (Fig. 1) the shapes of the differential GOS curves remain practically unchanged with the increase of the momentum transfer q by 2 orders of magnitude. The reason for this striking phenomenon is related to the localization of the 1*s* electrons. Specifically, the Ne 1*s* electrons (I_{1s}=32.77 a.u.) are localized near the nucleus within the radius range $r_{1s} \sim (2I_{1s})^{-1/2} \sim 0.12$ a.u. Thus, the integral, Eq. (2), will be non-negligible only if the radial continuum wave function, $P_{kl}(r)$, has appreciable amplitude in this region. For this Ne 1*s* case, the continuum wave functions, $P_{kl}(r)$, are negligible, in the region occupied by the 1*s* electrons for $l > 1$ for the secondary electron energies being considered, owing to the angular-momentum barrier [41]. Therefore, the primary contribution to the sum, Eq. (5), arises from the matrix elements of electron transitions from the 1*s* atomic state into the *s* and *p* continuua. However, for $q \leq 1$ the Bessel function $j_0(qr_{1s}) \approx 1$ and the electron transitions to the *s* state of the continuum are suppressed because of the orthogonality of the wave functions $P_{1s}(r)$ and $P_{k0}(r)$. Hence, the main contribution to the sum, Eq. (5), is made only by the dipole transition to the continuum and, according to Eq. (9), the confinement resonance behavior in the GOS is defined by the dipole amplitude factor $D_1(k)$ only. Furthermore, by these arguments, it is clear that for momentum transfer $q \leq 1$ the differential GOS and associated confinement resonances for Ne 1*s* will not change with q as seen in Fig. 1. With the increase of

momentum transfer, q, the situation changes somewhat. First, in the dipole channel, $j_1(qr_{1s})$ is no longer just $\sim qr_{1s}$; it becomes oscillatory in the region occupied by the $1s$ electron and, thereby, the integral, Eq. (2), becomes much smaller owing to the cancellation engendered by the oscillatory behavior. In addition, the contribution of the monopole $s \rightarrow s$ channel no longer vanishes because the approximation $j_0(qr_{1s}) \approx 1$ is no longer valid; but it is significantly smaller than the dipole contribution. So, as exemplified for the $q = 10$ a.u. case shown in Fig. 1, the magnitude of the differential GOS for Ne $1s$ is far smaller than the corresponding cases for lower q. In addition, the confinement resonance patterns differ slightly from the lower q cases owing to the presence of the monopole channel. The contribution of all the other transitions is negligible as before since the angular-momentum barrier does not allow the continuum waves to penetrate in the $1s$ region, irrespective of the momentum transfer.

A rather different picture is exhibited for ionization of the $2s$ level of the Ne atom with (ionization potential $I_{2s} = 1.93$ a.u.) shown in Fig. 2. This occurs because the Ne $2s$ wave function is significantly more diffuse than the $1s$ wave function by a factor of 5 or so. This means that except for very near the optical edge (very small q), where all contributions to the GOS, except the dipole contribution, vanish [30], there are a number of partial waves contributing to the $2s$ differential GOS, Eq. (5). Thus, while the Ne $2s$ confinement resonance structure for $q=0.1$ a.u. is determined only by the dipole term $[D_1(k)$ for the bubble potential], for larger values many more partial waves come into play; the most important being the $s \rightarrow d$ transitions. The dipole contribution still dominates for the small ejected electron energies considered, but the other terms are no longer negligible. This is seen for $q=1$ and 10 a.u. in Fig. 2, where the confinement resonance structures differ from each other and from the $q = 0.1$ a.u. case, as a function of secondary electron energy, for both potential models. In addition, for Ne $2s$, the shapes of the differential GOS differ substantially with momentum transfer q, owing to the different contributions of the various partial waves arising from the dependence of the oscillatory behavior of the spherical Bessel functions on q. In any case, for both $1s$ and $2s$ ionization of Ne by fast charged particles, it is clear that for low energy ejected electrons, the confining cage alters the differential GOS significantly.

Note that the energy and angular distributions of the fast (primary) electron are simply proportional to the differential GOS [30]. Thus, the confinement resonances exhibited in the differential GOS, discussed above, will also be seen in the energy and angular distribution of the scattered electron when viewed as a function of energy. Integrating over the angular distribution gives the single differential cross section, $d\sigma_{nl_0}/d\varepsilon$ [Eq. (6)], which involves an integral over the momentum transfer. Since the positions of the confinement resonances depend upon q, the confinement resonances will be somewhat diminished in the single differential cross section. But certainly, the importance of the confinement resonances near threshold should be exhibited since this was evident for all values of q.

As an example, the calculated single differential cross sections, $d\sigma_{nl_0}/d\varepsilon$, for the ionization of the $1s$ and $2s$ ground states of Ne confined in a C_{60} cage by incident electrons with kinetic energy $T=p_1^2/2=8$ keV are shown in Fig. 3, where it is seen that the cross sections of Ne from Ne@C_{60} are dramatically different both in magnitude and shape from the free Ne atom over the whole energy range ε under consideration. As previously, the details of the results for the bubble potential model and the spherical square-well model of the fullerene shell potential are different, with the amplitudes of the oscillations for the spherical square-well potential being smaller. The results for both potentials, nevertheless, are qualitatively identical. Since the endohedral resonances in the $1s$ case comparatively weakly depend on the transferred momentum, the resonance structure of the single differential cross section practically repeats the differential GOS confinement resonance structure seen in Fig. 1.

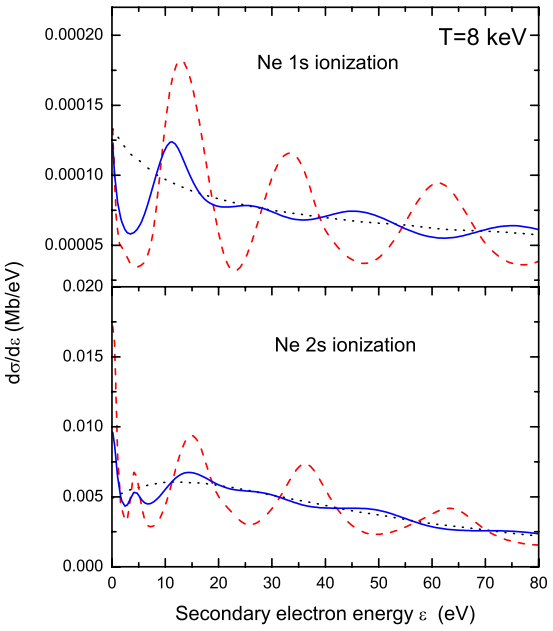

FIG. 3. (Color online) Single differential cross sections calculated for the ionization of $1s$ and $2s$ Ne subshells in Ne@C_{60} by electrons with incident kinetic energy $T=8$ keV using two different models of the cage potential—the bubble potential (dashed line) and the spherical square-well potential (solid line). Also shown is the calculated result for free Ne atoms (dotted line).

V. PLASMON EXCITATION OF C_{60}

Up to this point the potential of the fullerene shell $U(r)$ has been considered as static. This approximation is no longer valid when the energy transferred by fast charged particle to endohedral atom is close to the energy of the plasma oscillations of the delocalized C_{60} valence electrons. In this case the atomic ionization process induced via coupling with the C_{60} excitations will compete with the process of direct electron ionization from the atom A and in some cases even dominate.

For an atom at the center of a fullerene cavity, the delocalized C_{60} electrons localized in a spherical layer with thickness Δ and a mean radius R can be considered as electrons of an additional shell of atom A. Therefore, the inter-

action of the C_{60} electrons with the electrons of the encapsulated atom can be described similarly to the intershell interaction in a multielectron atom. In first order of this interaction the amplitude of the endohedral atom impact ionization (a matrix element of the Coulomb interaction of the fast electron with the electrons of the both shells) can be written as

$$M = \langle \mathbf{p}_1, \varphi_i^a | V_{12} | \mathbf{p}_2, \varphi_f^a \rangle - \sum_{E_i^C \le F, E_f^C > F} \frac{\langle \mathbf{p}_1, \varphi_i^C | V_{13} | \mathbf{p}_2, \varphi_f^C \rangle \langle \varphi_f^C, \varphi_i^a | V_{23} | \varphi_i^C, \varphi_f^a \rangle}{E_i^C - E_f^C + \Delta E} + \sum_{E_i^C \le F, E_f^C > F} \frac{\langle \mathbf{p}_1, \varphi_f^C | V_{13} | \mathbf{p}_2, \varphi_i^C \rangle \langle \varphi_i^C, \varphi_i^a | V_{23} | \varphi_f^C, \varphi_f^a \rangle}{E_i^C - E_f^C - \Delta E + i\eta}. \tag{13}$$

Here the first item is the amplitude of atomic impact ionization in the PWBA and the second and third ones define the intershell interaction between the electrons of the atom and C_{60}. The wave functions $|\mathbf{p}_1\rangle$ and $|\mathbf{p}_2\rangle$ in Eq. (13) are the plane waves describing the fast primary electron, and $|\varphi_i^C\rangle$ and $|\varphi_f^C\rangle$ are the wave functions of the C_{60} electrons with energies E_i^C and E_f^C, respectively. The summation in Eq. (13) over E_i^C is performed over the initial states of the C_{60} electrons occupying all the energy levels up to the Fermi energy F. The summation over E_f^C is performed on all the excited states of C_{60} including the integration over continuum states; the infinitesimal η shows the way around the pole. In the Coulomb interaction operators $V_{ij}=|\mathbf{r}_i-\mathbf{r}_j|^{-1}$, the vectors $\mathbf{r}_i$ are the radius vectors defining the coordinates of the fast primary electron ($\mathbf{r}_1$), the secondary electron ejected from the atom ($\mathbf{r}_2$), and an electron delocalized on the fullerene shell ($\mathbf{r}_3$).

The radius of the localization region of an inner shell of the atom A is of order $r_2 \sim (2I_{nl_0})^{-1/2} \ll 1$, while the radius of electrons on the fullerene shell are approximated equal to the mean radius, i.e., $r_3 \sim R \gg 1$. Thus, to an excellent approximation, the operator for the Coulomb interaction of electrons of these two shells is

$$V_{23} \approx \frac{1}{R} - \frac{(\mathbf{r}_2 \cdot \mathbf{r}_3)}{R^3}. \tag{14}$$

Because of the orthogonality of the atomic wave functions, only the second term in Eq. (14) results in nonzero matrix elements in the sums, Eq. (13). Thus, the Coulomb interaction, Eq. (14), is factorized by the dipole operators acting separately on the electrons of the atom A and fullerene C_{60}, respectively. The next orders of the expansion are responsible for the electron transitions of higher multipolarity; quadrupole, octupole, etc. We will not consider them here, restricting ourselves to the lowest-order (and most important) term in the expansion. From the dipole selection rules it follows that the second and third terms in Eq. (13) are different from zero only when the orbital moment of ejected electron is $l=l_0 \pm 1$. Therefore, in the sums for the partial amplitudes defining the SDCS, Eq. (1), and the GOS, Eq. (5), the intershell interaction influences the terms with the quantum number $\lambda=1$ only. These dipole partial amplitudes are then rewritten as

$$Q_{l_0 l}^1(q) = \langle nl_0 | j_1 | kl \rangle - \frac{\langle nl_0 | d | kl \rangle}{R^3} \alpha_d^g(q, \Delta E). \tag{15}$$

Here $\langle nl_0|d|kl\rangle$ is the dipole matrix element,

$$\langle nl_0 | r | kl \rangle = \int_0^\infty P_{nl_0}(r) r P_{kl}(r) dr, \tag{16}$$

and the function

$$\alpha_d^g(q, \Delta E) = \sum_{E_i^C, E_f^C} \left[\frac{\langle \varphi_i^C | j_1 | \varphi_f^C \rangle \langle \varphi_f^C | d | \varphi_i^C \rangle}{E_i^C - E_f^C + \Delta E} - \frac{\langle \varphi_i^C | d | \varphi_f^C \rangle \langle \varphi_f^C | j_1 | \varphi_i^C \rangle}{E_i^C - E_f^C - \Delta E + i\eta} \right] \tag{17}$$

is the generalized dynamic polarizability of the fullerene shell. This polarizability differs from the usual dynamic polarizability of C_{60} by the fact that in it one of the dipole matrix elements $\langle \varphi_i^C | d | \varphi_f^C \rangle$ is replaced by the matrix element of the Bessel function. In the optical limit ($q \to 0$) we obtain the relation of the generalized polarizability to the usual dynamic polarizability

$$\alpha_d(\Delta E) = \frac{3}{q} \alpha_d^g(q, \Delta E)_{q \to 0}. \tag{18}$$

For the same limit the dipole partial amplitude, Eq. (15), is written as

$$Q_{l_0 l}^1(q) = \langle nl_0 | j_1 | kl \rangle - q \frac{\langle nl_0 | d | kl \rangle}{3R^3} \alpha_d(\Delta E). \tag{19}$$

If the Bessel function is expanded also in the first term of Eq. (10) we get

$$Q_{l_0 l}^1(q) = \frac{q}{3} \langle nl_0 | d | kl \rangle \left[1 - \frac{\alpha_d(\Delta E)}{R^3} \right]. \tag{20}$$

Thus, in the optical limit, the dipole partial amplitude for impact ionization of the endohedral atom, to within a factor of $q/3$, coincides with the dipole photoionization amplitude for this atom, taking into account the dynamic interaction with the delocalized electrons of the fullerene shell [27,42]. The screening function

$$F(\Delta E) = \left[1 - \frac{\alpha_d(\Delta E)}{R^3} \right] \tag{21}$$

is a function of photon energy in the case of endohedral atom photoionization (in the impact-ionization case it is a function of transferred energy) and is characterized by rapidly changing behavior, especially for small ΔE. Therefore, for a range of energy transfer, the screening factor, Eq. (21), will significantly alter the dependence of generalized (and optical) oscillator strengths as a function of energy transfer, ΔE.

The screening function, Eq. (21), can be obtained either on the basis of model of the fullerene shell (such a method was used in [27]) or by using experimental data on the cross section for C_{60} photoabsorption [42]. Making use of the ana-

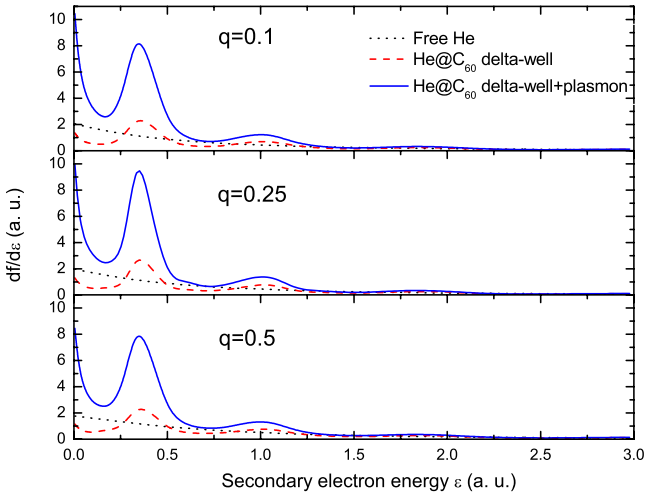

FIG. 4. (Color online) Differential generalized oscillator strengths calculated for ionization of He $1s$ of He@C_{60} as a function of ejected electron energy for several values of the momentum transfer q (in a.u.): solid line—bubble potential model including interaction with C_{60} plasmon, dashed line—static bubble potential. Also shown is the calculated result for free He atoms—dotted line.

lytical expression for this function [27] where the fullerene shell is simulated by a thin metallic sphere, the screening function has the form

$$F(\omega) = \frac{\omega^4 + \omega^2\Gamma_1^2}{(\omega_1^2 - \omega^2)^2 + \omega^2\Gamma_1^2}. \tag{22}$$

Here $\omega_1 \approx 20-22$ eV is the energy of the giant dipole (plasmon) resonance of C_{60} and $\Gamma_1 \approx 10-15$ eV is the width of this resonance.

Near the threshold for $1s$ ionization of endohedral He, the transferred energy is $\Delta E \geq I_{1s} \approx 25$ eV. Consequently, at the threshold of the process, where $\Delta E = \omega \sim \omega_1$, the factor, Eq. (22), increases the amplitude of dipole partial impact-ionization amplitude by approximately a factor of 4 and the partial ionization cross section by a factor of 16. With increasing energy transfer, corresponding to increasing kinetic energy of secondary electron, ε, the function, Eq. (22), rapidly goes to unity and so there is no influence on the GOS of the confined atom.

The differential GOS for the ionization of the $1s$ of confined He, calculated within the bubble potential model for several values of the momentum transfer q, is given in Fig. 4. In these calculations the width of the C_{60} giant dipole resonance is taken as $\Gamma_1 = 12$ eV; for this value of Γ_1 the photoabsorption cross section of a small metallic sphere [27]

$$\sigma^m(\omega) = \frac{4\pi N_e}{c} \frac{\omega^2\Gamma_1}{(\omega_1^2 - \omega^2)^2 + \omega^2\Gamma_1^2} \tag{23}$$

is close to experiment [33]. In Eq. (23) c is the speed of light and $N_e = 240$ is the number of delocalized electrons of C_{60}.

As seen from the figure, the effect of the coupling with the C_{60} plasmon excitation is to dramatically increase the amplitudes of confinement oscillations in the differential GOS near the electron ejection threshold. With the increase of energy transfer, the effect of the plasmon on the GOS on the process decreases and by $\Delta E \sim 2$ a.u. (54 eV) the effects of the plasmon can be neglected, which indirectly confirms the reasonability of applying in the case of the $1s$ and $2s$ Ne subshells the static approximation for the potential $U(r)$.

Note we considered the interaction of the electronic subsystems of atom and C_{60} shell in the dipole channel only. It is possible that plasmons of higher multipolarity generated by a fast charged particle also influence the impact-ionization process of the confined atom. Moreover, though the next (quadrupole) term of expansion, Eq. (14), is by a factor of r_2/R times less than dipole, its contribution to the amplitude of the process for energy transfer of the order of the quadrupole resonance energy could be of significance, but less important than the dipole correction, owing to the r_2/R term. In addition, there is a complete absence of any reliable information on plasmon resonances of C_{60} of higher multipolarity. For these reasons, they are not considered.

VI. IMPACT IONIZATION OF EMPTY C_{60} SHELL

Within the framework of PWBA the total cross section of impact ionization is associated with the photoionization cross section via an asymptotic expansion known as the Bethe-Born expansion [30,43,44]. Using this idea, along with Eq. (23), the total cross section for impact ionization of C_{60} can be obtained. The relation connecting these cross sections has the form

$$\sigma_{\text{tot}}(T) = \frac{1}{2\pi\alpha T} \int_0^{T-I} \frac{\sigma^m(\varepsilon)}{I+\varepsilon} \ln\left(\beta \frac{4T}{I+\varepsilon}\right) d\varepsilon. \tag{24}$$

Here $\varepsilon = \omega - I$ is the kinetic energy of the ejected (secondary) electron, α is the fine-structure constant, I is the C_{60} ionization potential, and β is a constant defining the upper limit of integration over momentum transfer. In the case of an atomic target, this constant is $\beta \sim 1/a_0$ (a_0 is the Bohr radius). Substituting the cross section, Eq. (23), in Eq. (24), we obtain for the total cross section for charged-particle impact ionization of C_{60},

$$\sigma_{\text{tot}}(T) = \frac{2N_e\Gamma_1}{T} \int_0^{T-I} \frac{I+\varepsilon}{[\omega_1^2 - (I+\varepsilon)^2]^2 + (I+\varepsilon)^2\Gamma_1^2} \times \ln\left(\beta \frac{4T}{I+\varepsilon}\right) d\varepsilon. \tag{25}$$

The calculated total cross section is shown for different values of the parameter β in Fig. 5. Also shown for comparison is the experimental data [23] and the PWBA results obtained within a spherical jellium shell model to describe the C_{60} electron states φ_i^C [26]. The parameter β is a characteristic feature of the Bethe-Born approximation, but it only enters logarithmically [29,30]. For high kinetic energies $T \gg I+\varepsilon$ the presence of the parameter β having the value of $\sim 1/R = 1/6.64$ within the logarithm is insignificant. Therefore, for high electron energy our results almost coincide with each other and they are seen to be close to experiment. For low energy our results prove to be much closer to experiment than the earlier semiempirical [25] or PWBA result [26]. The

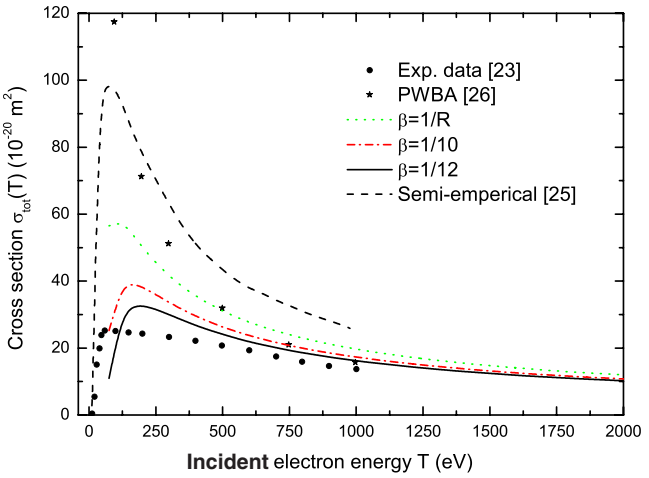

FIG. 5. (Color online) Total cross section for electron-impact ionization of C_{60} as a function of incident electron energy. Full circles—experimental data [23]; dashed line—semiempirical model calculation [25]; asterisks—previous PWBA results [26]; full curves—present Bethe-Born results for several values of β; see text for details.

basic reason for this is that the Bethe-Born calculation is based upon the photoionization cross section, Eq. (23), with parameters chosen to reproduce the experimental photoabsorption cross section of C_{60} [33]. Such an approach to the problem allows one to avoid explicit calculation of the discrete and continuum C_{60} electron wave functions.

VII. CONCLUSIONS

Fast charged-particle impact ionization of endohedral atoms has been studied and, using the s subshells of $Ne@C_{60}$ as a case study, it is found that confinement resonances abound for low-energy electron emission, just as they do for photoionization. The situation is somewhat more complicated in the charged-particle case owing to the fact that all partial waves are allowed, although the higher ones are negligible at the lower ejected electron energies owing to the angular-momentum barrier [41]. Two different models for static potentials are used to describe the effect of the C_{60} cage on the $Ne@C_{60}$ impact ionization. This is appropriate for the following reasons. First, comparing results within the two models provides insight into the dependence of confinement resonances on the thickness of the C_{60} potential well. While the results within the two models are found to be qualitatively the same, the spherical square-well potential predicts resonances that are of smaller amplitudes that die out more rapidly (with energy) as compared to the bubble potential. Second, while the finite-thickness square-well potential model seems to be more realistic compared to the bubble model, the latter has certain advantages since, being semianalytical, it provides a clearer qualitative understanding of behavior of confinement resonances in impact-ionization spectra of atoms confined inside C_{60}.

The static model potentials employed to simulate the effects of the C_{60} cage on the confined atom are approximate and do not give a complete description of charged-particle impact-ionization spectra in case the transferred energy ΔE proves to be comparable to the C_{60} plasmon oscillation energy, ω_1. The impact ionization of the He atom in the molecule $He@C_{60}$ which has been considered is an excellent example of this case. It was shown that the effect of the C_{60} dipole plasmon oscillation on the spectrum of secondary electrons is also great, just as in the case of low energy photoionization of endohedral atoms [16,45]. Moreover, like the photoionization case, the enhancement is also related to the dynamical polarizability of C_{60}, at least for small momentum transfer. For threshold secondary electrons the differential GOS is increased by more than an order of magnitude owing to the coupling with the C_{60} plasmon. Unlike dipole photoionization, impact ionization can be accompanied by the generation of plasma oscillations in C_{60} in nondipole channels, i.e., resulting from higher order terms in the expansion of the Coulomb interaction between shell and atomic electrons that are neglected in Eq. (4). Thus, if there are significant nondipole plasma oscillations in C_{60}, the impact-ionization cross section for endohedral atoms, for energy transfer close to the resonance energies of these oscillations, could be affected significantly. Further investigations, that we hope are stimulated by this paper, are needed to clarify this situation.

ACKNOWLEDGMENTS

This work was supported by DOE, Division of Chemical Sciences, Office of Basic Energy Sciences, Office of Energy Research, NASA, NSF, CAU CNFM, and Uzbek Foundation Award No. ΦA-Φ4-Φ095.

[1] Y. Chai, T. Guo, C. Jin, R. E. Haufler, L. P. F. Chibante, J. Fure, L. Wang, J. M. Alford, and R. E. Smalley, J. Phys. Chem. **95**, 7564 (1991).
[2] L. Dunsch and S. Yang, Small **3**, 1298 (2007).
[3] W. Harneit, C. Boehme, S. Schaefer, K. Huebener, K. Fostiropoulos, and K. Lips, Phys. Rev. Lett. **98**, 216601 (2007).
[4] M. A. G. Jones, J. J. L. Morton, R. A. Taylor, A. Ardavan, and G. A. D. Briggs, Phys. Status Solidi B **243**, 3037 (2006).
[5] C.-Y. Shu, X.-Y. Ma, J.-F. Zhang, F. D. Corwin, J. H. Sim, E.-Y. Zhang, H. C. Dorn, H. W. Gibson, P. P. Fatouros, C.-R. Wang, and X.-H. Fang, Bioconjugate Chem. **19**, 651 (2008).
[6] K. B. Hartman, L. J. Wilson, and M. G. Rosenblum, Mol. Diagn. Ther. **12**, 1 (2008).
[7] M. J. Puska and R. M. Nieminen, Phys. Rev. A **47**, 1181 (1993).
[8] G. Wendin and B. Wästberg, Phys. Rev. B **48**, 14764 (1993).
[9] P. Decleva, G. De Alti, G. Fronzoni, and M. Stener, J. Phys. B **32**, 4523 (1999).

[10] J.-P. Connerade, V. K. Dolmatov, and S. T. Manson, J. Phys. B **33**, 2279 (2000).
[11] M. Ya. Amusia, A. S. Baltenkov, V. K. Dolmatov, S. T. Manson, and A. Z. Msezane, Phys. Rev. A **70**, 023201 (2004).
[12] V. K. Dolmatov, A. S. Baltenkov, J.-P. Connerade, and S. T. Manson, Radiat. Phys. Chem. **70**, 417 (2004).
[13] M. Ya. Amusia, A. S. Baltenkov, and L. V. Chernysheva, Phys. Rev. A **75**, 043201 (2007).
[14] H. R. Varma, P. C. Deshmukh, V. K. Dolmatov, and S. T. Manson, Phys. Rev. A **76**, 012711 (2007).
[15] S. Lo, A. V. Korol, and A. V. Solov'yov, J. Phys. B **40**, 3973 (2007).
[16] M. E. Madjet, H. S. Chakraborty, and S. T. Manson, Phys. Rev. Lett. **99**, 243003 (2007).
[17] H. Katayanagi, B. P. Kafle, J. Kou, T. Mori, K. Mitsuke, Y. Takabayashi, E. Kuwahara, and Y. Kubozono, J. Quant. Spectrosc. Radiat. Transf. **109**, 1590 (2008), and references therein.
[18] A. Muller, S. Schippers, M. Habibi, D. Esteves, J. C. Wang, R. A. Phaneuf, A. L. D. Kilcoyne, A. Aguilar, and L. Dunsch, Phys. Rev. Lett. **101**, 133001 (2008).
[19] P. Scheier, B. Dunser, R. Worgotter, D. Muigg, S. Matt, O. Echt, M. Foltin, and T. D. Märk, Phys. Rev. Lett. **77**, 2654 (1996).
[20] S. Matt, B. Dunser, M. Lezius, H. Deutsch, K. Becker, A. Stamatovic, P. Scheier, and T. D. Märk, J. Chem. Phys. **105**, 1880 (1996).
[21] M. Foltin, O. Echt, P. Scheier, B. Dunser, R. Worgotter, D. Muigg, S. Matt, and T. D. Märk, J. Chem. Phys. **107**, 6246 (1997).
[22] M. Vos, S. A. Canney, I. E. McCarthy, S. Utteridge, M. T. Michalewicz, and E. Weigold, Phys. Rev. B **56**, 1309 (1997).
[23] V. Foltin, M. Foltin, S. Matt, P. Scheier, K. Becker, H. Deutsch, and T. D. Märk, Chem. Phys. Lett. **289**, 181 (1998).
[24] V. Tarnovsky, P. Kurunczi, S. Matt, T. D. Märk, H. Deutsch, and K. Becker, J. Phys. B **31**, 3043 (1998).
[25] H. Deutsch, K. Becker, J. Pittner, V. Bonacic-Koutecy, S. Matt, and T. D. Märk, J. Phys. B **29**, 5175 (1996).
[26] S. Keller and E. Engel, Chem. Phys. Lett. **299**, 165 (1999).
[27] J.-P. Connerade and A. V. Solov'yov, J. Phys. B **38**, 807 (2005).
[28] H. Bethe, in *Handbuch der Physik*, edited by H. Geiger and K. Sheel (Springer-Verlag, Berlin, 1933), Vol. 24, p. 273.
[29] L. D. Landau and E. M. Lifshitz, *Quantum Mechanics, Non-Relativistic Theory* (Pergamon, Oxford, 1965).
[30] M. Inokuti, Rev. Mod. Phys. **43**, 297 (1971).
[31] *Handbook of Mathematical Functions*, edited by M. Abramowitz and I. A. Stegun (Dover, New York, 1965).
[32] E. Tosatti and N. Manini, Chem. Phys. Lett. **223**, 61 (1994).
[33] J. Berkowitz, J. Chem. Phys. **111**, 1446 (1999).
[34] M. Ya. Amusia and A. S. Baltenkov, Phys. Rev. A **73**, 062723 (2006).
[35] L. L. Lohr and S. M. Blinder, Chem. Phys. Lett. **198**, 100 (1992).
[36] A. S. Baltenkov, Phys. Lett. A **254**, 203 (1999).
[37] A. S. Baltenkov, J. Phys. B **32**, 2745 (1999).
[38] M. Ya. Amusia, A. S. Baltenkov, and B. G. Krakov, Phys. Lett. A **243**, 99 (1998).
[39] M. Ya. Amusia and L. V. Chernysheva, *Computation of Atomic Processes* (IOP, Bristol, Philadelphia, 1997).
[40] V. K. Dolmatov and S. T. Manson, J. Phys. B **41**, 165001 (2008).
[41] A. R. P. Rau and U. Fano, Phys. Rev. **167**, 7 (1968).
[42] M. Ya. Amusia and A. S. Baltenkov, Phys. Lett. A **360**, 294 (2006).
[43] H. Bethe, Ann. Phys. **397**, 325 (1930).
[44] M. J. Seaton, Phys. Rev. **113**, 814 (1959).
[45] M. Ya. Amusia, A. S. Baltenkov and L. V. Chernysheva, JETP Lett. **87**, 200 (2008).